Optimized BSI CMOS Pixel for both UV and Visible Light

N. Fassi[1,2], J.-P. Carrère[1], M. Estribeau[2] , F. Omeis[1], E. Leon Perez[1], K. Jouannic[1], M. Orru[1], C. Augier[1], T. Combier[1], C. Blanc[1], A.S. Sodjo[1], P. Magnan[2] and V.Goiffon[2]
1. STMicroelectronics, 850 rue Jean Monnet, 38926, Crolles, France
2. ISAE-SUPAERO, Université de Toulouse, 10 av Edouard Belin, 31055, Toulouse, France
Email : {nour.fassi, jean-pierre.carrere}@st.com { magali.estribeau, pierre.magnan, vincent.goiffon}@ isae-supaero.fr

***Abstract*—This study proposes a comprehensive solution to the challenges to make a high-performance CMOS Image sensor for ultraviolet (UV) light, by utilizing backside-illuminated (BSI) CMOS image sensors with high-k antireflective coatings (ARC). It is first demonstrated that the backside interface electrical configuration allows an excellent draining of the photo generated carriers towards the photodiode. Next, the ARC layers initially optimized for visible (VIS) light show too strong absorption into UV. Finally, a new ARC stack has been defined by optical simulation. Experimental results next demonstrate that these optimized ARC configurations enhance the sensor's Quantum Efficiency (QE) in the UV range without compromising dark current or other performance metrics, making it suitable for wide-spectrum, high-resolution imaging applications.**

***Key words*—ultraviolet, backside illuminated pixels, CMOS image sensors, quantum efficiency, interface defects, antireflective coatings, high-k dielectric.**

I. INTRODUCTION

Ultraviolet imaging opens new industrial applications such as transparent material sorting and skin blemish monitoring in healthcare. The UV wavelength range of interest lies between 200 to 400 nm, as shown in Figure 1.

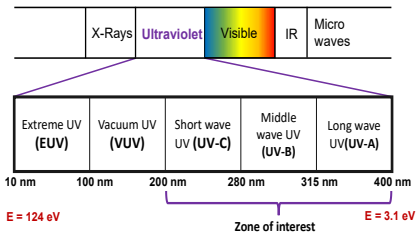

Fig. 1 UV wavelength range of interest for this study

Designing an image sensor with a good response in this range presents several challenges. Firstly, the layers above the photodiode must be transparent to these wavelengths, which limits the choice in terms of materials that can be used as anti-reflective coating [1]. This is one of the reasons why BSI image sensors are beneficial for UV applications.

Secondly, as illustrated in Figure 2, due to their energy, these photons are absorbed very close to the silicon surface, within just a few tens of nanometers. Therefore, the quality of the silicon interface must be particularly well-maintained to prevent the recombination of carriers generated so close to the surface.

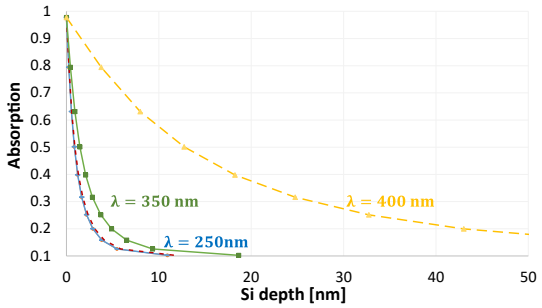

Fig. 2 Beer-Lambert law in silicon showing a very short penetration depth of the UV light, about 10nm for λ=200nm. [1]

Various solutions to drive the photogenerated charge away from the interface have already been proposed: creating an electric field that moves carriers away from the interface by doping the near-interface region, as depicted in the zoomed in backside interface in Figure 3, using implantation doping and laser annealing[2], or later by delta-doping techniques [3].

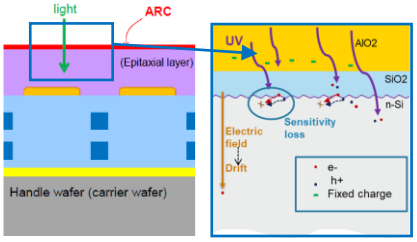

Fig. 3 Backside Illumination pixel configuration, and a zoom on the interface, showing the challenges for UV sensing: photon absorption into ARC, recombination of the generated carriers due to interface defects.

This study focuses on the fabrication of a wide-spectrum CMOS image sensor utilizing BSI N-type pixels adapted to small pitch, including a vertical Pinned Trench Photo MOS [4] and high-k ARC.

It will first describe the experimental setups to measure the performances, simulate both the electrical and optical behaviors of the backside part to understand the responses of the sensor under UV and then, it will detail the steps to optimize the sensor for UV, showing it's QE results, compared to the literature.

II. EXPERIMENTAL

The CMOS image sensor studied here uses BSI N-type 4T pixels adapted to small pitch, including a vertical Pinned Trench Photo MOS [4] and high-k ARC. The sensor does not include colour filter nor microlens. The pixel pitch is around one micron, and the pixel MOS transistors are typical of the 40 nm technology node. They are isolated from each other

by a deep and conductive trench (CDTI), allowing the depletion of a deep photo-collection area. Charge transfer to the readout node is ensured by a Vertical Gate (VEGA) (Figure 4). Their configuration incorporates high-k dielectrics that exhibit a negative fixed charge, enabling electrical passivation of the interface by hole filling and creates an electric field that drifts photoelectrons away from the interface (Figure 4).

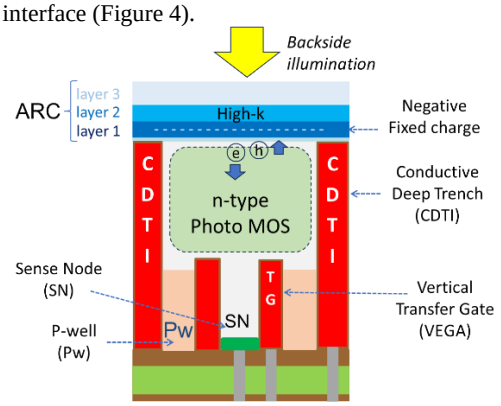

Fig. 4 The studied n-type pixel is a vertical Pinned Trench Photo MOS [4].

The QE of the pixels was measured in this study using two different test benches adapted for UV imaging. The first one allows the measurement of the response at the chip level, utilizing a deuterium lamp and bandpass filters. The second measures the response at the wafer level, using a xenon source, a monochromator, a liquid light guide, and lenses adapted to UV. Both setups allow characterization down to the wavelength of 250 nm.

III. ANALYSIS OF THE BSI PIXEL QE IN UV

A. *Quantum Efficiency measurements*

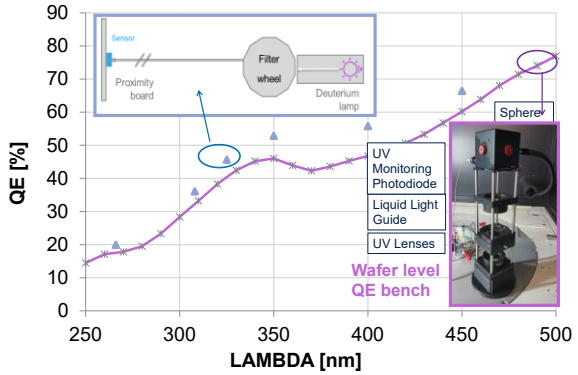

Fig. 5 Quantum efficiency of the monochrome BSI pixel under UV light.

Figure 5 shows the QE of the reference pixel of this study, a standard monochrome photogate technology sensor, measured on both experimental setups. These measurements show good agreement and an observable UV response down to 250 nm. The QE is higher than 70% for blue light at 450 nm but decreases down to 15% at 250nm. As expected, this reference pixel is more suited for visible than UV wavelength. We propose a way to optimize them to reach a higher QE in the UV range.

B. *Backside electrical simulations*

The measured QE is the product of the Charge Collection Efficiency (CCE) and the transmission of the superficial layers. The first step consisted in determining, thanks to simulations, which one of these parameters may be the cause of the QE drop in the UV range. A previous study [5] showed that the electrical charge of high-k dielectrics is sufficient to create an electric field higher than 10^5 V/cm. This field results in a drift velocity of photogenerated charges around 10^5 cm/s, making recombination phenomena at the interface negligible, with typical recombination velocities of about 300 cm/s [6]. Thus, the CCE of the pixel should approach 100%, which cannot explain the observed QE drop in the UV range. (Figure 6).

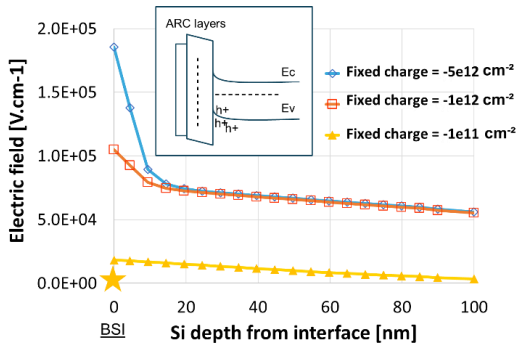

Fig. 6 TCAD simulation of the electric field at backside interface, for different negative fixed charges quantity in the ARC. The star being the start of limitation between the dielectric and the Si

C. *Optical simulations*

Optical simulations have been performed with *Lumerical FDTD* to analyze the UV absorption in the superficial layers. Figure 7, first, compares the QE at the die level with the simulated QE.

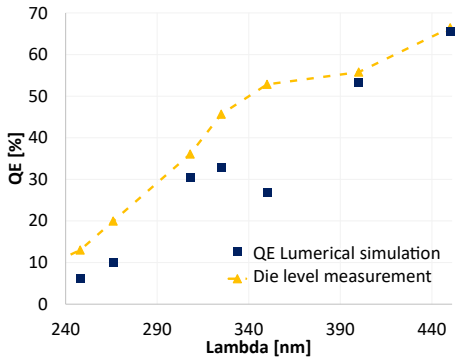

Fig. 7 Comparison between the experimental QE of the n-type BSI pixel under UV light and the optical simulation of the external QE by Lumerical FDTD

Figure 8 shows that the ARC layer 2 has a very strong absorption at 200nm indicating the main cause of the loss of photons in the UV range.

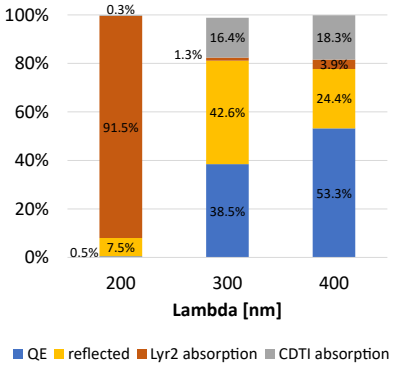

Fig. 8 Optical simulation of the photons' loss in the pixel Vs lambda

IV. BACKSIDE ARC OPTIMIZATION FOR UV

The high absorption seen in Figure 8 is consistent with the optical extinction coefficient under UV observed for the layer 2 in Figure 9. This figure shows also alternative materials like HfO_2 [8].

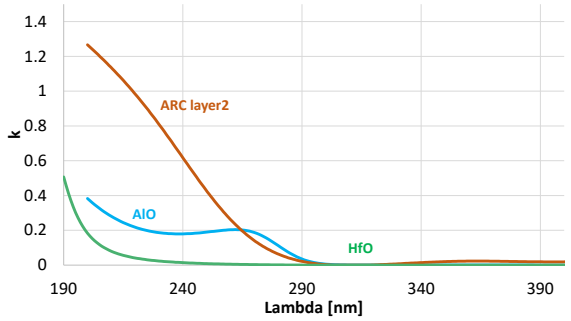

Fig. 9 Ellipsometry measurement of the optical k coefficient vs the UV wavelength for different High-k materials. It confirms the UV-A absorption in the layer 2.

Optimal ARC layer properties for both UV and visible light have been determined by optical simulation, based on different combinations of high k dielectrics showing low UV absorption. The configurations giving the best simulated QEs have then been fabricated. They are shown, as well as the reference original non adapted BSI pixel (sample 1) in figure 10. These UV-adapted ARC are all based on HfO and contain three or five layers.

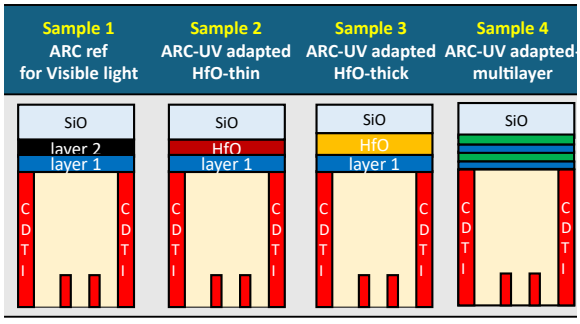

Fig. 10 Description of the elaborated BSI pixels with UV adapted ARC based on HfO, with 3 layers or 5 layers configurations

Figure 11 shows the optical simulation of the total transmission thorough the different ARC, where a clear increase of the transmission is observed under 300nm with the new ARC configurations.

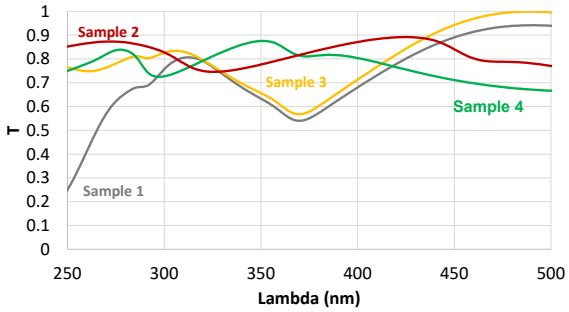

Fig. 11 Optical simulation of the total transmission thorough the different ARC.

The QE and dark current performances of each of these optimized pixels have been characterized. The optimized ARC configurations (sample 2 to sample 4) (figure 12), demonstrate significant improvements in QE for both UV and visible light.

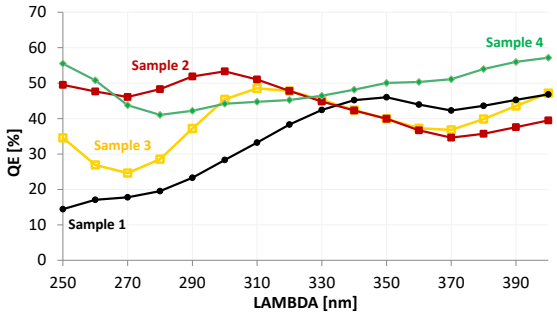

Fig. 12 QE measurement under UV of optimized pixels compared to the reference one.

The five-layer stack (sample 4) exhibited superior performance across the remaining UV range without impacting, in most cases, the QE in visible light.

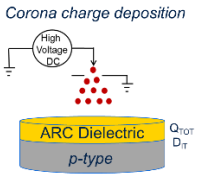

ARC	Dit [1/cm²*eV]	Qtot [1/cm²]
Ref ARC - sample 1	2.0E+11	-2.0E+12
ARC UV adapted - 3 layers	2.0E+11	-1.9E+12
ARC UV adapted - 5 layers	2.2E+11	-2.0E+12

Fig. 13 ARC fixed charge and interface defects density measurement by Corona discharge tool

The aim of this new development was also to modify the ARC without deteriorating the backside interface passivation performances and, by extension, without increasing the dark current. The new ARC dielectric fixed charge and interface states density were evaluated using the Corona method [7], and no significant change was found (Figure 13), indicating that the good passivation performance of the backside interface should be maintained.

	1-ARC ref for Visible light	2-ARC-UV adapted HfO-thin	3-ARC-UV adapted HfO-thick	4-ARC-UV adapted multilayer
CVF (µV/e)	120	120	120	120
PRNU @ 2ke-	<1%	<1%	<1%	<1%
FPN	<1e-	<1e-	<1e-	<1e-
Temporal Noise (e)	<2e-	<2e-	<2e-	<2e-
Full Well (e)	>8000	>8000	>8000	>8000
relative Idark (a.u.)	1.0	1.1	0.9	0.9
QE_520nm(%)	85	67	86	69
QE_400nm(%)	47	40	47	57
QE_300nm(%)	28	56	40	47
QE_250nm(%)	14	42	37	49

TABLE I MAIN PERFORMANCE SUMMARY OF THE SAMPLE WITH MODIFIED ARC

Finally, the optimized ARC configurations did not significantly change the dark current or any main pixel performance values. Table 1 shows that no regression on dark current or noise was observed and that a good PRNU and the QE response in visible are maintained as well as an improvement in the QE on UV.

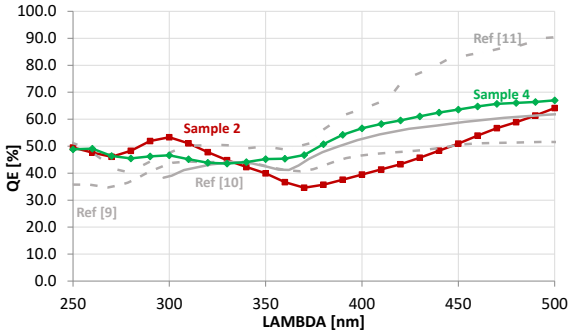

Fig. 14 QE result from UV to visible of the better performing modified BSI pixels compared to literature

Additionally, the modified N-type BSI pixel demonstrated promising performance with QE of 40-50% in UV, compared to in-market small-pitched BSI CIS technologies, showing that these pixels are at the state of the art (Figure 14).

V. CONCLUSION

The optimized ARC configurations developed in this study significantly enhance the QE of BSI CMOS image sensors across the UV spectrum while maintaining the already good response in the visible spectrum. These findings highlight the potential of several thin-layered multi-stacks in achieving high-efficiency image sensors, paving the way for further advancements in UV-sensitive pixel technology. Notably, the modifications preserved the passivation quality and did not increase the dark current, ensuring the sensor's overall performance. The improved performance of the modified N-type BSI pixel highlights its suitability for wide-spectrum, high-resolution imaging applications.

REFERENCES

[1] Fassi, N., Carrère, J. P., Magnan, P., Estribeau, M., & Goiffon, V. (2023). Quantum efficiency of backside-illuminated pixels under ultraviolet illumination: ARC coatings impact measurements and simulations. Electronic Imaging, 35, 1-5.

[2] Peng Sun, Sheng Hu, Wen Zou, Peng-Fei Wang, Lin Chen, Hao Zhu, Qing-Qing Sun, and David Wei Zhang , "Backside passivation for improving the noise performance in CMOS image sensor", AIP Advances 10, 045229 (2020) https://doi.org/10.1063/5.0006700

[3] Hoenk, Michael & Jones, Todd & Dickie, Matthew & Greer, Frank & Cunningham, Thomas & Blazejewski, Edward & Nikzad, Shouleh. (2009). Delta-doped back-illuminated CMOS imaging arrays: Progress and prospects. Proceedings of SPIE-The International Society for Optical Engineering. 7419. 10.1117/12.832326.

[4] Roy, F., Suler, A., Dalleau, T., Duru, R., Benoit, D., Arnaud, J., ... & Lu, G. N. (2020). Fully depleted, trench-pinned photo gate for CMOS image sensor applications. *Sensors*, *20*(3), 727.

[5] Fassi, N., Carrère, J. P., Perez, E. L., Estribeau, M., Magnan, P., & Goiffon, V. Analysis of Backside Illuminated CMOS pixels' Quantum Efficiency under Ultraviolet Illumination. *tic*, *1*, 2.

[6] Eades, W. D., & Swanson, R. M. (1985). Calculation of surface generation and recombination velocities at the Si-SiO2 interface. Journal of applied Physics, 58(11), 4267-4276.s, W. D., & Swanson, R. M. (1985). Journal of applied Physics, 58(11), 4267-4276.

[7] Sacchettini, Y., Carrère, J. P., Doyen, C., Duru, R., Courouble, K., Ricq, S., ... & Magnan, P. (2019, December). A highly reliable back side illuminated pixel against plasma induced damage. In *2019 IEEE International Electron Devices Meeting (IEDM)* (pp. 16-5). IEEE.

[8] Vereecke, B., Cavaco, C., De Munck, K., Haspeslagh, L., Minoglou, K., Moore, G., ... & Osman, H. (2015). Quantum efficiency and dark current evaluation of a backside illuminated CMOS image sensor. *Japanese Journal of Applied Physics*, *54*(4S), 04DE09.

[9] Sony IMX487, IMX661(July 2022)

[10] Hoenk, M. E., Jewell, A. D., Kyne, G., Hennessy, J., Jones, T., Cheng, S., ... & Skottfelt, J. (2022, August). 2D-doped silicon detectors for UV/optical/NIR and x-ray astronomy. In X-Ray, Optical, and Infrared Detectors for Astronomy X (Vol. 12191, pp. 354-373). SPIE.

[11] XIMEA, Gpixel: PulSar. December 2023